Project IMPART

Integrated Modeling and Prediction of Atmospheric Reentry Trajectories

Max Heil

Dr. Kumar

AE 5626: Orbital Mechanics for Engineers

December 12, 2024

THE OHIO STATE UNIVERSITY

COLLEGE OF ENGINEERING

1 Introduction

In recent years, engineers have seen a drastic increase in objects orbiting the Earth. Satellites are one of the most common space objects, as they play a crucial role in communication, navigation, and observation of life on Earth. However, their operational lifetimes are limited and require careful consideration for end-of-life planning. Many times, this means performing a controlled reentry back into the atmosphere to burn-up satellite components. Predicting where, when, and how the satellite will break up is critical to the safety of human life and to mitigate further debris accumulation. This problem is ever-growing and has relevant implications on our daily lives. Just as recently as March 8, 2024, a piece of space debris from the International Space Station (ISS) hit a home in Naples, Florida.

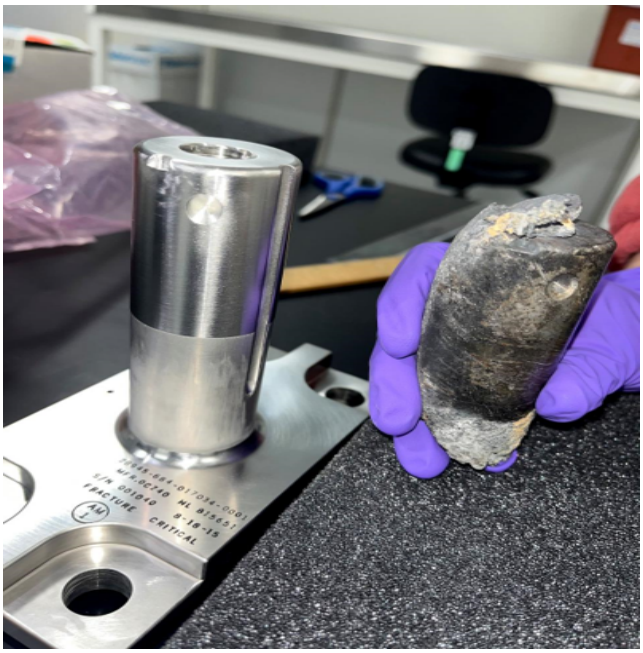

Figure 1: A stanchion from the NASA flight support equipment used to mount ISS batteries on a cargo palet survived reentry and collided with a home in Naples, Florida on March 8, 2024 [1]

Predicting the decay of a satellite's orbit over time and the impact footpoint of reentering space objects is inherently complex due to fluctuations in atmospheric density, thermal ablation, dynamic drag coefficients, and much more. Various institutions have investigated both theoretical and empirical models to advance prediction methods.

Most methods of predicting the reentry process use separate models for each phase. The first step in reentering the atmosphere is to decrease the size of your orbit. This phase is called orbit decay. The primary method used to estimate orbit decay comes from the mean motion or King-Hele theory. This theory is based on the circularization, or contraction of the orbit, due to atmospheric drag [2]. A principle assumption of this theory is that perigee height remains constant. This allows us to define the orbital lifetime in terms of mean motion, n, where a value of n (chosen by the user) represents an "end value" of circular height. For example, a value of $n = 16.5$ rev/day would correspond to a circular altitude of 150 km [2]. The only values that are not directly observed from orbital data to be used in the calculation of orbital decay are the drag coefficient, C_D, and density, ρ, as will be discussed in the analysis section.

Once the orbit has been lowered and circularized, the object will begin to enter the lower atmosphere where more external forces must be considered. Figure 2 gives a generalized view of a potential path the object can take after entry. This part of the atmosphere is typically where most satellites begin to breakup due to an excess of drag causing extreme heating. Additionally, aerodynamic and gravity forces must be decomposed into components to account for uneven particle distributions. A set of first order nonlinear ODE's developed by Wilbur L. Hankey from Wright State University is widely used for this type of low-fidelity 3DOF dynamics simulations [3]. Higher order models are used commercially, but are unavailable to the public at large.

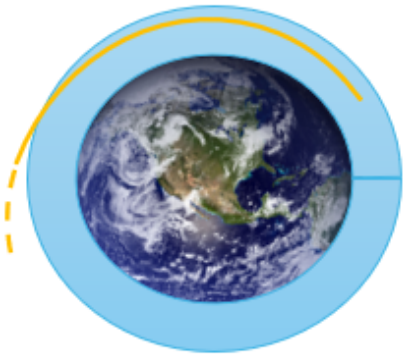

Figure 2: Initial atmospheric entry occurs around 80 to 100 km

The final phase of reentry is impact. Approximately 40% of a satellite will have survived the initial atmospheric breakup phase and continue to impact [2]. During this phase, the satellite debris will span velocities over the entire flight regime ($0 < M < 25$). This nonlinearity demands a large ground footprint zone for potential debris trajectories. Of the three phases, this phase is with out a doubt the hardest to predict. That is why engineers will typically expand impact footprints to account for unexpected debris that could have survived reentry. A Monte Carlo simulation environment is one of the best ways to generate ground impact distributions. Using a Kernel Density Estimation (KDE) technique to create a smooth 2D Probability Density Function (PDF) for a given scenario returns promising results with relatively low error [4]. However, this estimation method can require thousands of simulation runs and a "computer farm" to complete the simulations in a reasonable amount of time.

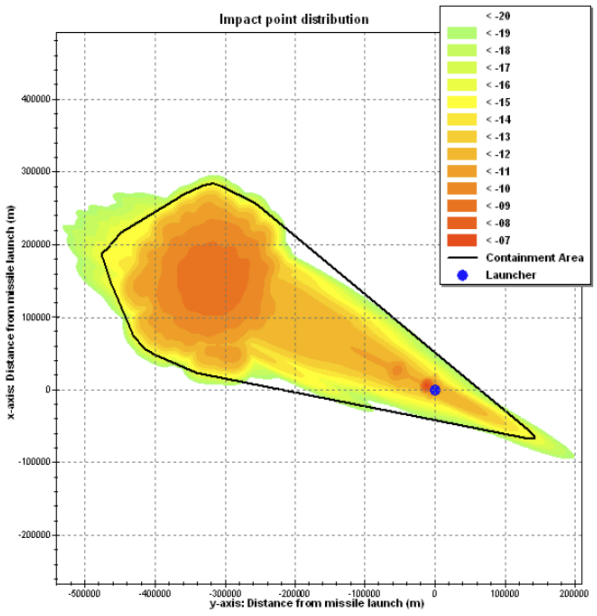

Figure 3: Example of ground impact PDF ($\log_{10}$ scale) [4]

2 Problem Statement

While I had initially hoped to complete a full, low-fidelity computational analysis of reentry events that included orbit decay, initial reentry, and impact footprint predictions, a lack of time and resources required a pivot in direction. However, my overall problem statement remains the same. I seek to address the challenges of predicting satellite reentry trajectories and impact by developing a robust, physics-based simulation framework. The framework should incorrporate the following:

1. Gravitational and atmospheric models
2. A model for orbit decay above 100 km altitude
3. Dynamic equations of motion for reentry, including aerodynamic forces and gravity
4. Probabilistic and numerical techniques such as Monte Carlo, Runge_Kutta, and ode113

This project is meant to be a glimpes into estimation and the parameters that go into predicting satellite reentry trajectories. I include a discussion of my own challenges with this project in later sections.

3 Methodology

The methodology employed for this project follows a similar structure to the existing literature I discussed earlier, tailored to address the challenges of modeling satellite reentry. This section outlines the step-by-step approach used to simulate the reentry events, including plans for those steps unable to be completed.

The reentry events were broken up into three phases: orbit decay, atmospheric reentry, and impact footprint. This was done so that each part could be modeled separately and stitched together for analysis.

All code and figures for this project were written/produced in MATLAB® R2022a and Simulink. Several built-in toolboxes were used and I discuss those in their respective sections.

3.1 Modeling Orbit Decay

To begin, we need to setup the framework for the gradual reduction in altitude due to atmospheric drag (formally called orbit decay). First, let's consider the acceleration due to drag given by the equation below,

$$\boldsymbol{a_{drag}} = -\frac{1}{2}\frac{C_D A}{m}\rho V_A^2 \boldsymbol{v} \tag{1}$$

where C_D is the drag coefficient, A is the aerodynamic effective cross-section area, m is the satellite mass, ρ is the local neutral density of the atmosphere, V_A^2 is the satellites relative airspeed, and $\boldsymbol{v}$ is the unit vector in the direction of the relative airspeed. Note that the drag acceleration is a *vector* with scalar coefficients. To further expand this equation, we can define relative airspeed and unit vector to be:

$$V_A = |\boldsymbol{V} - \boldsymbol{\omega_e} \times \boldsymbol{r}| \tag{2}$$

$$\boldsymbol{v} = (\boldsymbol{V} - \boldsymbol{\omega_e} \times \boldsymbol{r}) \tag{3}$$

with $\boldsymbol{\omega_e}$ being 2π rad/day and $\boldsymbol{V}$ being the satellite's inertial velocity vector.

Under a high-fidelity assumption, C_D would be variable with time since it can change with temperature, density, exposed surface area, and more. Thus, for my modeling purposes, I will assume that C_D is a constant throughout the duration of flight. Equation 4 represents the ballistic coefficient that is created from this assumption (which will also remain constant).

$$B^* = \frac{C_D A}{m} \tag{4}$$

However, density will not be constant during the orbital decay phase. While the change is not too significant at high altitudes, it does have a big impact in determining trajectories. Thus, there needs to be a suitable model to estimate the density at a given altitude to accurately determine the atmospheric drag.

There are several advanced atmospheric density and temperature models that exist. The Mass Spectrometer and Incoherent Backscatter (MSIS) model and the Thermospher/Ionosphere General Circulation Model (TIGCM) are some of the most accurate. These models incorporate semi-analytical and semi-empirical solutions to reduce overall error. The TIGCM model has even reported standard deviations as low as $\pm$ 8.98% in March of 1979 [5]. Relative to a simplistic isothermal analytical density model, as shown in Eq. 5, this is considered to be groundbreaking. Later, in the results section, we will see actual values for how improved the advanced models are.

$$\rho = \rho_0 e^{-\frac{z}{H}} \tag{5}$$

For the simple model, ρ_0 represents the density at sea-level, z is the height above the surface, and H is the scaled height. This model may be advantageous for some cases, since it provides an approximation with little computational consumption. The high-fidelity models will account for solar flux, geomagnetic index, and diurnal, monthly, and seasonal variations, but are computationally intensive. A simple simulation can take several hours to complete on an 8GB RAM, 64-bit hardware system.

The only solution for modeling density in the aerodynamic acceleration due to drag equation is to find a built-in model in MATLAB®. Luckily, the Naval Research Laboratory MSIS model has a built in function called `atmosnrlmsise00` that takes inputs of current altitude, latitude, longitude, epoch date, and UT time and outputs the current density and temperature for that location in space. This density model is sufficient for altitudes above 100 km, but has the potential to break down past $\sim$ 450 km.

Now that we have considered decelerations from drag, we need to also consider the other major force at high altitudes: gravity. For this, it is reasonable to use Newton's universal law of gravitation which is the foundation of the two body problem (TBP). This assumption is valid because we are only considering the Earth and the satellite in our system. In this case μ_e is the Earth's gravitational constant.

$$\ddot{\boldsymbol{r}}_g = \boldsymbol{a}_g = -\frac{\mu_e}{r^3}\boldsymbol{r} \tag{6}$$

More sophisticated models, such as the zonal harmonics model which captures perturbations based on the non-uniformity of Earth (EGM2008), could replace a TBP assumption to more accurately compute the gravitational acceleration [6]. However, with the time constraints and precision of this project, I felt the simple gravitational model was best for high altitudes.

Now that we have the necessary accelerations accounted for, we can simply add them to get our overall acceleration for the orbital decay phase. Equation 7 shows this below.

$$\boldsymbol{a}_{total} = \boldsymbol{a}_g + \boldsymbol{a}_{drag} \tag{7}$$

Each of these models (density, gravity, and drag), were placed in their own functions for easy accessibility. To compute the derivatives of the state vector for orbital motion, the total acceleration and velocity were calculated from the current state such that,

$$\boldsymbol{x} = \begin{bmatrix} \boldsymbol{r} \\ \boldsymbol{v} \end{bmatrix}, \quad \dot{\boldsymbol{x}} = \begin{bmatrix} \boldsymbol{v} \\ \boldsymbol{a} \end{bmatrix} \tag{8}$$

where $\boldsymbol{r} = [r_x \;\; r_y \;\; r_z]^T$ and $\boldsymbol{v} = [v_x \;\; v_y \;\; v_z]^T$. Equation 8 along with the initial state vector are numerically integrated using MATLAB's ode113. This numerical integration provides the evolution of the state vector over time in the ECI frame.

3.2 Modeling Reentry

The reentry phase is assumed to begin after we have hit 100 km of altitude. The transition from the orbit decay model to the reentry model will occur at this time. As in the orbital simulator, we must find accurate values for density, temperature, and other atmospheric properties. Once again, I will employ the NRMLSISE-00 density function mentioned in the previous section for atmospheric prediction.

As the satellite approaches the ground, the nonuniform shape of Earth becomes more of a factor. Thus, our gravitation model from the decay phase must be improved to account for this. These perturbations effects are accounted for in the term J_2 which is a zonal coefficient that when considered, the gravity vector remains in the plane containing the satellite position vector and the north pole [7]. We can break this vector up into two components. The first component acts in the direction opposite of the position vector, call this $\vec{e}_r$. The second component is perpendicular to the position vector, call this $-\vec{e}_\phi$. Therefore, the gravity vector becomes,

$$\boldsymbol{g} = -g_r \boldsymbol{e}_r - g_\phi \boldsymbol{e}_\phi \tag{9}$$

The components g_r and g_ϕ are given in Eq. 10 and Eq. 11, respectively.

$$g_r = \frac{\mu}{r^2}\left[1 - \frac{3}{2}J_2\left(\frac{R_{earth}}{r}\right)^2\left(3\sin^2\phi - 1\right)\right] \tag{10}$$

$$g_\phi = \frac{3\mu J_2}{r^2}\left(\frac{R_{earth}}{r}\right)^2 \cos\phi \sin\phi \tag{11}$$

Clearly, the g_r component will be much larger than the g_ϕ component since most of the gravity will point in the radial direction (towards Earth's center). Note that the constants used for these equations are as follows: $\mu_e = 3.9865 \times 10^5$ km^3/s^2, $R_e = 6378.137$ km, and $J_2 = 1.08263 \times 10^{-3}$.

Now that we have a model created for reentry gravity, it is important to look at the other big force, which is the aerodynamic forces. Inside 100 km, it is necessary to decompose these forces into three main components. These components are referred to as drag, lift, and side force. Starting with the lift vector, this will act perpendicular to the velocity vector and will have the lowest affect on the body. The drag force will be most prevalent and will act opposite the direction of the velocity vector. Finally, the side for acts horizontally in the plane of motion. While we only considered drag during the decaying phase, all three will have a significant impact here. The equations for each are listed below.

$$D = \frac{1}{2}\rho(h)V^2 S C_D(\alpha, \beta, M) \tag{12}$$

$$L = \frac{1}{2}\rho(h)V^2 S C_L(\alpha, \beta, M) \tag{13}$$

$$Y = \frac{1}{2}\rho(h)V^2 S C_Y(\alpha, \beta, M) \tag{14}$$

The coefficients for each are non-dimensional and are functions of α and β, which are the satellite angle of attack and sideslip angle. The surface area of the satellite, up to this point, is referred to as S in these equations. As I mentioned in the orbit decay phase, a future extension of this project could include a model of these coefficients that incorporates α and β,

but due to similar reasons as before, I will assume they are constants[1].

Now that we have a model for the gravitational and aerodynamic forces, we need to incorporate them in equations of motion for state estimation. I used the following set of first order nonlinear ODE's for a low-fidelity 3DOF dynamic model (similar to orbit decay) [3].

$$\frac{dV}{dt} = -\frac{D}{m} - z_g \sin(\gamma) + x_g \cos(\gamma) + r\omega_e^2 \cos(\phi)\big(\cos(\phi)\sin(\gamma) - \sin(\phi)\sin(\psi)\cos(\gamma)\big) \tag{15}$$

$$\frac{d\gamma}{dt} = \frac{L}{mV} - \frac{z_g}{V}\cos(\gamma) + \frac{x_g}{V}\sin(\gamma)\sin(\psi) + \frac{V}{r}\cos(\gamma) + 2\frac{\omega_e}{V}\cos(\phi)\cos(\psi) + r\omega_e^2\big(\cos(\phi)\cos(\gamma) - \sin(\phi)\sin(\psi)\sin(\gamma)\big) \tag{16}$$

$$\frac{d\psi}{dt} = \frac{Y}{m\cos(\gamma)V} - \frac{V}{r\cos(\gamma)}\tan(\phi) + \frac{z_g}{V}\frac{\cos(\psi)}{\cos(\gamma)} + 2\frac{\omega_e}{V}\big(\sin(\psi)\cos(\phi)\tan(\gamma) - \sin(\phi)\big) \tag{17}$$

These equations of motions will change with velocity, flight path angle, and the satellite's heading as it heads towards the ground. The kinematic equations used to describe the vehicles position as it changes over time includes variables such as the altitude, latitude, and longitude. These kinematic equations are described below.

$$\frac{dr}{dt} = V\sin(\gamma) \tag{18}$$

$$\frac{d\phi}{dt} = \frac{V\cos(\gamma)\sin(\psi)}{r} \tag{19}$$

$$\frac{d\theta}{dt} = \frac{V\cos(\gamma)\cos(\psi)}{r\cos(\phi)} \tag{20}$$

Instead of using an ODE solver for this situation, my literature review strongly indicated that a Runge-Kutta solver is the best with integrating this system of equations. Therefore, I implemented a 4th order Runge-Kutta solver that I built in MATLAB® to integrate the system over the time of flight. Figure 4 demonstrates the process for trajectory prediction for the reentry phase of flight. At last, we have arrived at a predicted trajectory with a low-fidelity and computationally inexpensive model.

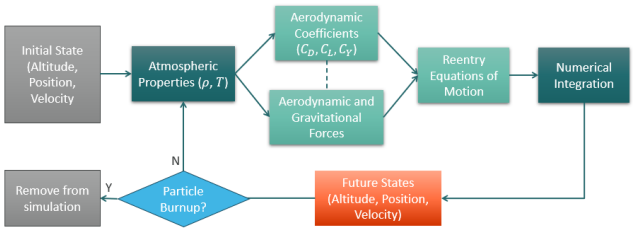

Figure 4: 3DOF simulation flowchart to be implemented into Simulink®

3.3 Modeling Impact (future)

The final step of this reentry event analysis would be to identify an impact footprint. Unfortunately, I was unable to get to this step due to struggles with finding converging solutions for the reentry phase. As I mentioned in the introduction, this project is a glimpse into the world of reentry and there is plenty of room for expansion in future work. Nonetheless, below is a general blueprint for which I would have follow, had I been able to complete this step:

1. Define initial conditions for debris, including velocity, flight path angle, heading, and altitude, with uncertainties.

2. Introduce random perturbations to account for variations in atmospheric density, aerodynamic forces, and fragmentation dynamics.

3. Simulate multiple trajectories using numerical integration to compute impact locations. Plot these locations on a 3D map to get an impact footprint.

4. Generate a probability density map of the impact footprint using KDE [4].

5. Validate the footprint against known events or high-fidelity models and refine as needed.

[1] I would also be interested to see how different the results really are if you include variations in the coefficients (maybe a future project!)

4 Results

The results presented in this section demonstrate the outcomes of the numerical simulations and analyses conducted for the reentry phases. These include the orbital decay, atmospheric reentry dynamics, and initial trajectory predictions. Each phase is analyzed to evaluate the effectiveness of the models and to identify areas for refinement. Although a final impact footprint simulation was not completed, intermediate results demonstrate plausibility for future analysis.

First, Fig. 5 illustrates the accuracy discovered when using the MSIS model in MATLAB® at low altitudes.

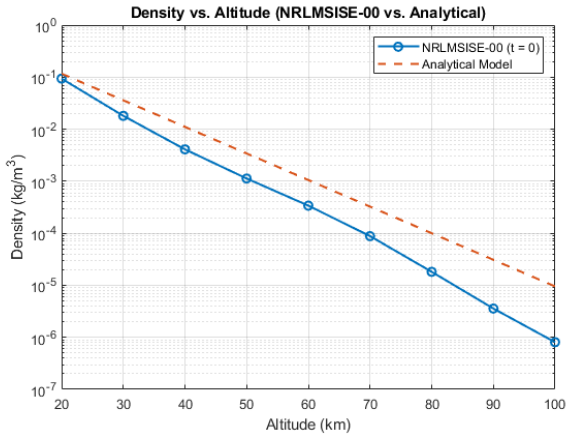

Figure 5: Accuracy of density model (MSIS) vs. the simplistic analytical model at low altitudes (Eq. 5)

Similarly, the MSIS model is much more accurate at high altitudes (Fig. 6).

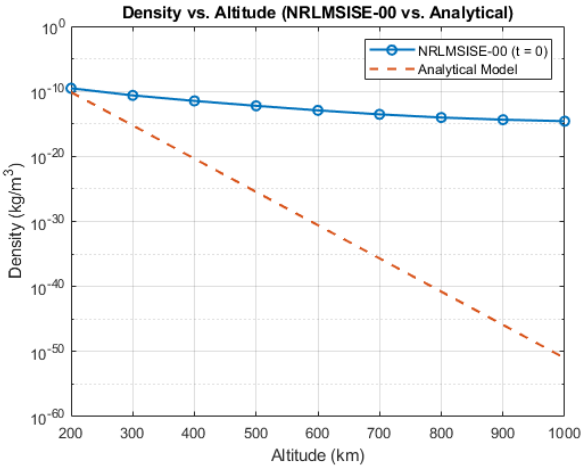

Figure 6: Accuracy of density model (MSIS) vs. the simplistic analytical model at high altitudes (Eq. 5)

Additionally, the orbital decay simulation showed promising results with a high mass satellite with the following parameters: initial altitude of 500 km, a simulation time of 2 days, a constant drag coefficient $C_D = 2.2$, an aerodynamic cross-sectional area of $A = 10\,\mathrm{m}^2$, and a mass of 1000 kg.

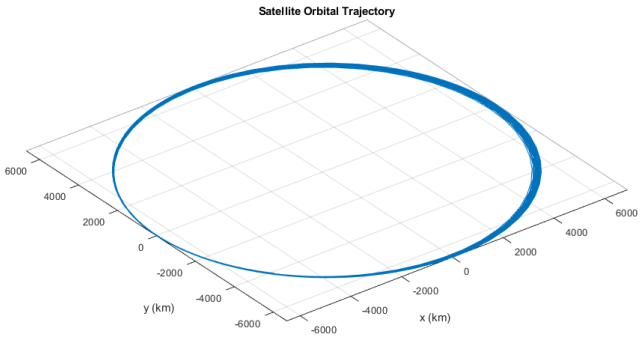

Figure 7: Visualization of the orbital decay over time in a 2D plane showing a decaying apogee and constant perigee. Simulator cut off at 100 km to switch to reentry simulator

The decaying apogee with the same parameters is seen in an altitude vs. time plot as well.

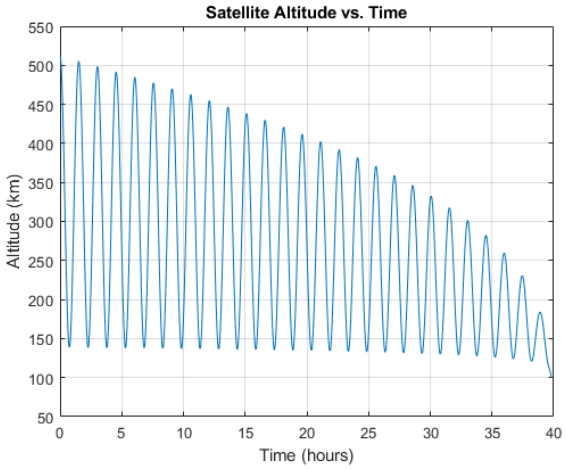

Figure 8: Satellite's altitude over time. The maximum altitude is the apogee and the minimum is the perigee

I was interested to see that when cutting the mass in half, this plot changes significantly. Figure 9 represents this plot.

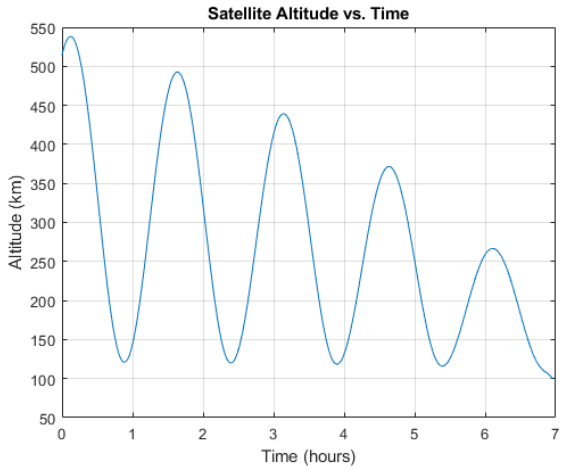

Figure 9: Satellite's altitude over time with the mass cut in half

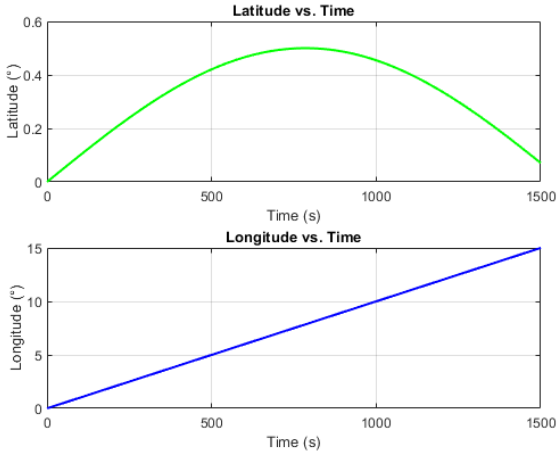

Figure 11: Latitude and longitude plots vs. time for reentry simulator

Finally, with a lower starting altitude of around 350 km and the same parameters to begin with, the following plot was found. Figure 10 illustrates an interesting concept in satellite reentry dynamics that will be discussed in the next section.

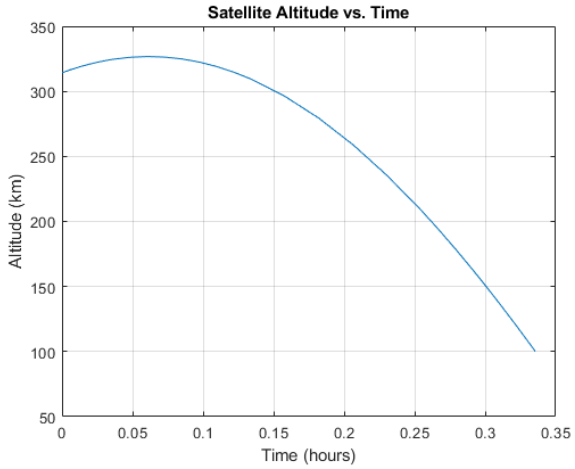

Figure 10: Satellite's altitude over time with the starting altitude at 350 km

When transitioning to the reentry simulation, I previously mentioned that I was getting either poor or non-converging results. The results were still plotted and compared for the sake of the project. Arriving at the correct results was not necessary the goal of the project (while it would have been nice), but I was able to at least get *some* results from this simulator. Figures 11 - 12 illustrate these results.

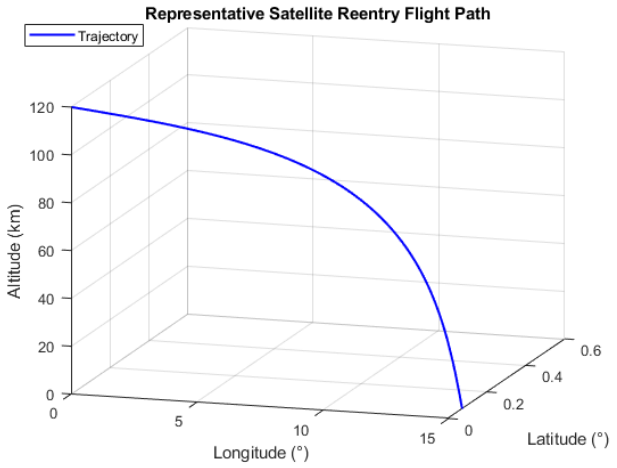

Figure 12: 3D flight path of reentry satellite

5 Discussion & Conclusion

Several key conclusions can be made from these illustrative results. First, Fig. 5 - 6 demonstrate the significant difference between an isothermal and empirical density model. Clearly the isothermal model falls apart at high altitudes and we have used a much more accurate density estimation.

In terms of the orbit decay simulator, I arrived at results that match the theory. Fig. 7 shows a decaying apogee, just as I had assumed would happen during the circularization process. Each period in orbit results in a slightly lower apogee height.

Figure 8 confirmed the results found in the 3D visualization plot. The satellite reduced altitude to 100 km in just under 40 hours. Additionally, the perigee (minimum) altitude re-

mained relatively constant while the apogee (maximum) altitude decreased with each frequency. It is worthy to note that right around 37 hours, there was a rapid decent in the apogee altitude as well. This is due to the increased drag experienced near 100 km.

When reducing the mass in Fig. 9 to 500 kg, we see that the change in perigee altitude after each pass becomes much greater than for a 1000 kg satellite. Additionally, reducing the mass caused a quicker decent of only 7 hours. This makes sense because mass is apart of our ballistic coefficient (Eq. 4) which is increased if mass is decreased, thereby increasing the overall drag and reducing the amount of time needed to decrease the apogee altitude.

Starting from a lower altitude and a 1000 kg satellite clearly caused a quick decent, as in Fig. 10. Again, the drag on the spacecraft is much greater at 350 km than 500 km. The object took less than 1 hour to decay to an altitude of 100 km. What is interesting is that the satellite was trying to overcome the drag initially, as evident by the maxima in the plot. I believe this to mean that we have achieved a somewhat optimal case since a slower, yet shorter decent means lower velocities and aerodynamic forces.

Finally, I will acknowledge the struggles associated with Figures 11 - 12. Clearly, these plots are undesirable and are not converging to correct results. I believe the error to be in the integration process, but with little time and resources I was unable to complete any troubleshooting.

Nonetheless, I think that I have completed my goal of laying the framework for a robust, physics-based trajectory estimation framework by incorporating a multi-phase approach to the reentry analysis. I have successful incorporated several atmospheric models along with aerodynamic and gravitational force models for each phase of reentry. Future work could include fixing the reentry model error, creating functions for the C_D, C_L, and C_Y coefficients, or completing the impact analysis and developing a full heating model for particle burn-up below 80 km. Overall, I think the work I have done in this project should excel anyone wanting to improve upon existing first order models of reentry dynamics.

5.1 Final Remarks & Acknowledgment

I greatly enjoyed working on this project and the MATLAB® code. I know this report is likely longer than 4 pages (sorry!), but I felt it was only necessary to explain every detail of my methodology, even if it was unsuccessful. This is an interesting topic and I hope to continue working with it in the future. Thank you for all your help this semester, Dr. Kumar, as I learned a bunch!

References

[1] L. David, "Uncontrolled reentry of space debris poses a real and growing threat," *Space News*, 2024.

[2] B. D. Neuenfeldt, "A survey of uncontrolled satellite reentry and impact prediction," Master's thesis, United States Naval Postgraduate School, 1993.

[3] A. Fedele, S. Omar, S. Cantoni, R. Savino, and R. Bevilacqua, "Precise re-entry and landing of propellantless spacecraft," *Advances in Space Research*, vol. 68, no. 11, pp. 4336–4358, 2021.

[4] S. Wilson, I. Vuletich, I. Bryce, M. Brett, W. Williams, D. Fletcher, M. Jokic, and N. Cooper, "Iac-09-d2.2.09 space launch & re-entry risk hazard analysis – a new capability," vol. 9, 01 2009.

[5] F. Marcos, R. Roble, and T. Killeen, "Thermosphere and ionosphere dynamics during 20–30 march 1979 time period: Comparison of tigcm calculated densities with observations," *Advances in Space Research*, vol. 12, no. 6, pp. 93–96, 1992.

[6] N. K. Pavlis, S. A. Holmes, S. C. Kenyon, and J. K. Factor, "The development and evaluation of the earth gravitational model 2008 (egm2008)," *Journal of Geophysical Research: Solid Earth*, vol. 117, no. B4, 2012.

[7] M. M. Peet, "Spacecraft Dynamics and Control." `https://control.asu.edu/Classes/MAE462/462Lecture13.pdf`, 2023. [Accessed 5-12-2024].